designs

MDPI

Article

Rheological Behaviour of ABS/Metal Composites with Improved Thermal Conductivity for Additive Manufacturing

Vicente F. Moritz [1,2,*], Harald Prévost [3], Janaína S. Crespo [4], Carlos A. Ferreira [2] and Declan M. Devine [1,*]

[1] PRISM Research Institute, Technological University of the Shannon, Dublin Rd., N37 HD68 Athlone, Ireland
[2] Postgraduate Programme in Mining, Metallurgical and Materials Engineering (PPGE3M), Federal University of Rio Grande do Sul (UFRGS), Bento Gonçalves Av. 9500, Porto Alegre 91509-900, Brazil; ferreira.carlos@ufrgs.br
[3] ENSIACET, Institute National Polytechnique de Toulouse, Emile Monso Rd., 31030 Toulouse, France; harald.prevost@gmail.com
[4] Postgraduate Programme in Materials Science and Engineering (PPGMAT), University of Caxias do Sul (UCS), Francisco Getúlio Vargas St. 1130, Caxias do Sul 95070-560, Brazil; jscrespo@ucs.br
* Correspondence: vicente.moritz@ufrgs.br (V.F.M.); declan.devine@tus.ie (D.M.D.)

Abstract: Metal-reinforced polymer composites are suitable materials for applications requiring special thermal, electrical or magnetic properties. Three-dimensional printing technologies enable these materials to be quickly shaped in any design directly and without the need for expensive moulds. However, processing data correlating specific information on how the metal particles influence the rheological behaviour of such composites is lacking, which has a direct effect on the processability of these composites through melt processing additive manufacturing. This study reports the compounding and characterisation of ABS composites filled with aluminium and copper particulates. Experimental results demonstrated that the tensile modulus increased with the incorporation of metal particles; however, there was also an intense embrittling effect. Mechanical testing and rheological analysis indicated poor affinity between the fillers and matrix, and the volume fraction proved to be a crucial factor for complex viscosity, storage modulus and thermal conductivity. However, a promising set of properties was achieved, paving the way for polymer–metal composites with optimised processability, microstructure and properties in melt processing additive manufacturing.

Keywords: polymer–matrix composites (PMCs); particle reinforcement; rheological properties; thermal properties; 3D printing

Citation: Moritz, V.F.; Prévost, H.; Crespo, J.S.; Ferreira, C.A.; Devine, D.M. Rheological Behaviour of ABS/Metal Composites with Improved Thermal Conductivity for Additive Manufacturing. *Designs* **2023**, *7*, 133. https://doi.org/10.3390/designs7060133

Academic Editor: Tiago Pinto Ribeiro

Received: 19 October 2023
Revised: 14 November 2023
Accepted: 16 November 2023
Published: 17 November 2023

1. Introduction

Polymer–metal composites are of particular interest for applications in which either thermal or electrical conductivity is required since polymers are not intrinsically conductive [1–6]. For instance, concern has arisen due to warpage and distortion caused by thermal expansion on polymer-based 3D-printed parts. Finite element analysis (FEA) simulations have been employed to model the mechanical and thermal behaviours of parts built through fused deposition modelling (FDM) [1,3,7]. Therefore, materials with improved thermal properties would address the final product's potential distortion in the fabrication of large-dimension structures such as electromagnetic interference shields and antennas [1]. A combination of heat dissipation and electrical insulation is usually desired in encapsulated electronic devices, preventing a potentially jeopardising overheating situation while enabling the retention of the electrical functionality [4,8]. Moreover, inserts for injection hybrid moulds (which are manufactured through 3D printing techniques) have also proven to benefit from inorganic fillers, exhibiting improved heat dissipation and greater longevity and yielding parts with properties comparable to those produced with conventional injection moulding [9–11]. In this context, metal-reinforced polymer–matrix composites have become an alternative material to overcome these issues as the addition

of fillers, either particles or fibres simply with conductivity greater than that of polymers, aimed at improving mechanical characteristics combined with light weight, can also impart distinct thermal, electrical, optical or magnetic properties to the material [5,7,12,13].

The effects of a number of conductive fillers on the properties of different polymer materials have been investigated, with particular emphasis on copper and aluminium powders, and various experimental approaches and numerical models have been employed to assess the thermal conductivity of such composites [14–20]. For instance, Rahmati and Dickens (2007) [21] and Pontes et al. (2008) [22] carried out studies on aluminium-filled 3D-printed epoxy inserts for hybrid moulds, evaluating the thermal and mechanical properties and reporting promising outcomes relative to enhancing the thermal performance of the moulds. Ranjan et al. (2023) [23] 3D-printed ABS parts to fabricate composites with aluminium metal spray reinforcement, and then applied machine learning methodologies to optimise the process variables and the flexural properties. Akrout et al. (2023) [24] investigated the structural, thermal, micromechanical and tribological properties of ABS/Cu composites for bearing applications. Compared to neat ABS, the composites showed a higher hardness and elastic modulus. Significant improvements in ABS's mechanical and thermal properties suggest that a suitable selection of material composition and other parameters may lead to a FDM filament of great potential, yielding high-performance, functional prototypes for a wide range of applications manufactured with the FDM process [7,25].

From the point of view of the material, the acrylonitrile–butadiene–styrene copolymer (ABS) is known for its excellent mechanical and impact strengths, dimensional stability, good chemical resistance, low water absorption and high filling capacity, arising as a popular thermoplastic material of choice for FDM applications as it offers satisfactory processability and a relatively low melting temperature [5,26–29]. The manufacturing of ABS composites through additive manufacturing (AM) techniques, such as FDM, has been demonstrated [30–34], and melt flow index (MFI) analysis has been a popular testing choice to evaluate the flow behaviour trends of ABS composites developed for 3D printing [35–41]. Isa et al. (2015) [35] and Sa'ude et al. (2016) [36] studied the behaviour of ABS/copper composites, and Kumar et al. (2019) [38] carried out similar work on ABS/aluminium composites, with all of them targeting the development of materials for extrusion-based AM processes; nonetheless, their results indicated that the filler has distinct effects on MFI depending on its content, suggesting that there would be no direct dependence between the loading content and MFI. However, only knowing a material's MFI is insufficient to process it, since this type of measurement represents the flow of a material under the pressure applied during its testing, and it does not encompass considerations due to shear conditions a polymer chain will be subjected to as it undergoes the processing stage [42–44]. Moreover, MFI lacks accuracy and reproducibility as it is a single-point viscosity value relative to the shear rate and applied pressure at a fixed temperature, prone to inherent measurement errors as well as experimental errors [44–46].

On the other hand, considering that the flowability of a polymer is inversely proportional to the dynamic viscosity, it is well known that the melt flow behaviour (MFB) is an important parameter for 3D printing as the printed parts' precision and interlayer adhesion may be affected by both the shear thinning effect (which determines the pressure needed to push the material through the nozzle) and the temperature parameters (which will ultimately govern the mechanical properties and integrity of the printed parts) [43,47–50]. Dynamic oscillatory rheometry has been employed to determine the appropriate processing conditions for high-performance thermoplastics in the form of AM feedstock, as it provides a more comprehensive rheological profile of such materials, such as including other linear viscoelastic properties of interest, e.g., melt storage modulus (G') and complex viscosity (η^*), and it has been successfully utilised to characterise ABS composites [51–57].

However, there is a gap of knowledge regarding the dynamic rheological properties of ABS/metal composites [58]. Within this frame of reference, this work aims to provide a better understanding of the effect of incorporating metallic particles on the rheological and viscoelastic properties of ABS, which is essential to determine the feasibility of these

polymer/metal compounds as potential candidates for thermally conductive thermoplastic composites' AM feedstock. In this study, metal particle-reinforced ABS composites were produced through extrusion compounding and injection moulding, with aluminium and copper particles incorporated into the polymer matrix. In addition, mechanical, rheological, viscoelastic, thermal and morphological characterisation techniques were employed to evaluate the effects of the metallic fillers' loadings on the composites' performance, as a suitable set of properties may be challenging to achieve, especially for highly loaded systems.

2. Experimental

2.1. Materials

Commercial-grade ABS was supplied by LG Chemical under trade name TR-557I as a transparent, impact-resistant material. Aluminium powder (250 mesh, >99.7%, air-atomised) and copper powder (325 mesh, >99.0%, water-atomised) were supplied by East Coast Fibreglass.

2.2. Metallic Powders Characterisation

Aluminium and copper powder were analysed in order to determine their surface and physicochemical properties, such as specific surface area, mean particle size and crystalline structure. Surface adsorption characteristics were studied in a Quantachrome Nova 1000e unit with nitrogen 5.0 as testing gas, and the specific surface area (A_{sp}) was calculated using the Brunauer–Emmett–Teller (BET) isothermal model. Laser scattering particle size distribution measurements were performed in a Horiba LA-950 granulometer. X-ray diffraction was carried out in a Siemens/Bruker D5000, with 2θ angle ranging from 10° to 80° at a $0.05^{\circ}\cdot s^{-1}$ step, utilising a Cu-$K\alpha$ tube (λ = 1.54056 Å).

2.3. Compounding and Extrusion

Metal-reinforced composites were prepared by mixing and extruding ABS with the metallic powders in a co-rotating twin-screw Leistritz Macromatex II (Ø 27 mm, 36:1 L/D ratio), with a temperature profile of 200–230 °C from the throat to nozzle at 30 rpm. Prior to compounding, ABS and metallic powders were dried at 80 and 110 °C, respectively, for 2 h. Following extrusion, obtained composites were pelletised. Composite formulations were designed with two variable factors at two levels; the polymer/metal weight ratios are presented in Table 1, along with the theoretical volume fractions of polymer, f_{ABS}, and the metal filler, f_{met}.

Table 1. Metal powder contents for the composites prepared.

	ABS [wt%]	Al [wt%]	Cu [wt%]	f_{ABS}	f_{met}
ABS-30%Al	70	30	-	0.855	0.145
ABS-60%Al	40	60	-	0.627	0.373
ABS-30%Cu	70	-	30	0.951	0.049
ABS-60%Cu	40	-	60	0.848	0.152

wt% = 100 × (phase mass)/(total mass).

2.4. Injection Moulding and Processing Optimisation

An Arburg 370E Allrounder injection moulding machine (Ø 30 mm screw) was utilised in this study with a temperature profile of 195–220 °C from the throat to nozzle. Composite pellets and virgin ABS were pre-dried at 70 °C for four hours. Specimens (ASTM D638 type I tensile, unnotched ASTM D6110 Charpy impact and Ø 25 mm disc) were moulded. Allowing for the increased viscosity due to the filler contents, the injection process parameters needed to be modified in order to reach an optimal moulding condition for each formulation (Table 2), preventing issues such as short shots and flashing.

Table 2. Injection moulding parameters employed for process optimisation.

	ABS	ABS-30%Al	ABS-60%Al	ABS-30%Cu	ABS-60%Cu
Injection Pressure [bar]	805	1050	1890	900	1070
Holding Pressure [bar]	500	500	1600	500	500
Mould Temperature [°C]	50 ± 5	50 ± 5	50 ± 5	50 ± 5	50 ± 5
Cooling Time [s]	30	30	45	30	30

2.5. Mechanical Testing

Stress–strain tensile tests were performed with injection-moulded ASTM D638 type I specimens in a Zwick Roell (Zwick GmbH & Co. KG, Ulm, DE) universal testing machine with a 10 kN loadcell and testXpert III (version 1.5) software by the same manufacturer, based on ASDM D638-14. Test speed was 5 mm·min^{-1}, and gauge length was 50 mm. A total of 16 specimens were tested for each formulation.

Unnotched Charpy impact test was carried out based on ASTM D6110-10 in a Ceast Resil 6844 (Ceast Instron SpA, Turin, Italy) digital machine with a 4.0 J hammer. Specimens were mechanically notched so that the material remaining in the specimen under the notch was 10.16 ± 0.05 mm thick. Twelve specimens were tested for each formulation. Hardness tests were carried out on a CV Instruments Shore D Durometer (CV Instruments Ltd., Sheffield, UK) digital machine, with a test load of 5.0 kg. A total of 64 measurements were taken from each sample. For both tests, the values reported were calculated as the average of the recorded values.

2.6. Dynamic Rheology

Oscillatory dynamic rheology of the composites was studied using a Discovery HR30 rheometer (TA Instruments, New Castle, DE, USA), featuring a parallel-plate geometry fixture with Ø 25 mm and 1.0 mm gap. To ensure that the strain utilised was within the linear viscoelastic region, amplitude sweep tests were performed within a strain range from 0.1% to 100% at 1.0 Hz. Frequency sweep experiments, also known as small angle oscillatory shear (SAOS), were carried out within a frequency range from 100 to 0.01 Hz under a strain of 1%. In SAOS studies, the flow curves follow a power law equation, $\eta^* = K \times \omega^n$, that expresses the shear thinning parameter n, which provides a semi-quantitative measurement of the filler dispersion [52,53]. Temperature of 195 °C and nitrogen atmosphere were applied for both test modes. Three specimens of each formulation were analysed in each testing mode.

2.7. Dynamic Mechanical Thermal Analysis

Dynamic mechanical analysis (DMA) was used to investigate the storage modulus (E') and the glass transition temperature (T_g). A DMA Q800 (TA Instruments, New Castle, US) machine was used for the analysis using single cantilever mode with a free bending length of 17.5 mm. The specimens were 12 mm wide and 2 mm thick. A 1 µm oscillation amplitude, 1 Hz oscillation frequency and 5 °C·min^{-1} heating rate from room temperature to 160 °C were employed. Three specimens of each material were analysed. T_g was determined as the $tan(\delta)_{DMA}$ peak temperature.

2.8. Thermal Conductivity

The thermal conductivity (k) of specimens was measured using a H111A Heat Transfer Unit (P.A. Hilton Ltd., Andover, UK). A disc specimen (Ø 25 mm, thickness 2 mm) was fitted between two parallel-plate copper blocks. A voltage and current of 80 V and 0.109 A were applied, and six specimens were tested. Finally, the surface temperatures were estimated according to the manufacturer's instructions, and k (for the materials) was calculated based on Fourier's Unidirectional Heat Transfer Law.

2.9. Scanning Electronic Microscopy

The morphology of the impact fracture surfaces was observed through a field emission scanning electron microscope (FE-SEM) (Tescan Mira 3, Tescan UK/Oxford Instruments, Cambridge, UK), with a 10 kV energy beam using the backscattered electrons (BSE) mode. Prior to analysis, specimens were mounted on a metallic stub and gold-coated for 30 s at 0.13 mbar vacuum. Combined with the FE-SEM instrument, a surface chemical composition mapping was carried out through energy dispersive spectroscopy (EDS) equipped with a silicon drift detector (SDD) to evaluate the dispersion of the metal particles within the ABS matrix.

2.10. Statistical Analyses

Analysis of variance (ANOVA), a statistical method, was employed to assess whether the metallic powder type and content were significant for the composites' properties. All the values were analysed at a 99% confidence interval, and differences were considered significant through the *p*-value test when $p \leq \alpha = 0.01$. In order to determine differences between sample groups, Tukey's HSD pairwise post hoc test was applied [11,59].

3. Results and Discussion

3.1. Physicochemical Properties of Metallic Powders

The aluminium and copper powder's specific surface areas were estimated through the BET model [60] and were 2.14 and 3.41 $m^2 \cdot g^{-1}$, respectively, which are very low values and indicate an absence of porosity. The granulometric distribution data are shown in Table 3. The metallic powders presented mean particle sizes of 27.95 ± 9.59 µm (Al) and 23.55 ± 9.92 µm (Cu), which are consistent with the differences in specific surface area and material density. Both powders demonstrated a unimodal frequency distribution of particle sizes (Figure 1), with ca. 63% of their particles within the medium silt range (14.5–28.5 µm). Aluminium had 30.16% of its particles falling within the coarse silt range, while copper presented a more balanced distribution between fine silt (19.09%) and coarse silt (16.46%). It is also important to mention that the powders were synthesised through distinct processes. The aluminium powder was produced through gas atomisation, a process that usually yields fine, regular and spherical particles, while copper powder was manufactured through water atomisation, which produces particles with highly irregular morphology [61,62]. The powders' synthesis is therefore likely related to both the specific surface area and the particle size distribution.

Table 3. Surface adsorption characteristics and granulometry distribution of the metallic powders.

		Aluminium	Copper
	Specific surface area	2.14 $m^2 \cdot g^{-1}$	3.41 $m^2 \cdot g^{-1}$
	Mean size ± SD	27.95 ± 9.59 µm	23.55 ± 9.92 µm
	Mode size	27.88 µm	21.41 µm
	Diameter on 10%	17.17 µm	13.34 µm
	Diameter on 50%	26.69 µm	21.69 µm
Diameter Frequency	Very fine silt (3.5–7.0 µm)	-	0.49%
	Fine silt (7.0–14.5 µm)	6.21%	19.09%
	Medium silt (14.5–28.5 µm)	62.98%	63.27%
	Coarse silt (28.5–57.0 µm)	30.16%	16.46%
	Very fine sand (57.0–115.0 µm)	0.64%	0.69%

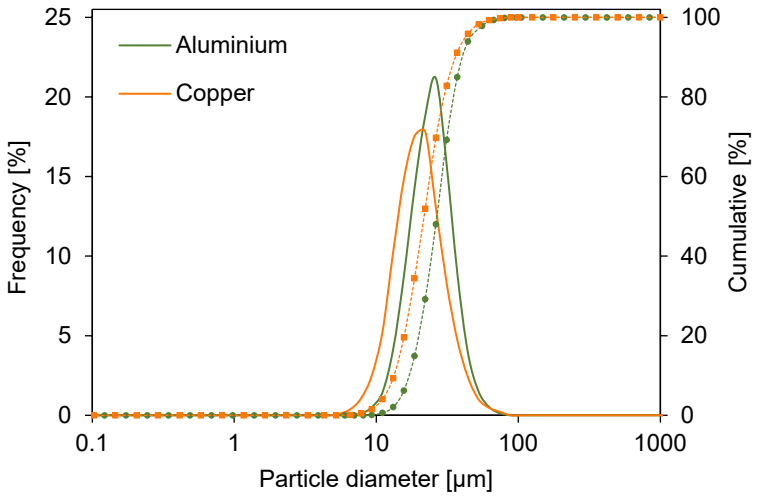

Figure 1. Frequency and cumulative distributions of particle sizes of aluminium and copper powders obtained with laser scattering granulometry. Frequency (solid line) and cumulative (dotted line) distributions of particle sizes obtained with laser-scattering granulometry.

The XRD patterns of both powders are presented in Figure 2. The powder diffraction data were processed with Rietveld refinement using the GSAS-II software [63]. Both aluminium and copper powders were found to match the diffraction patterns for pure metallic phases recorded on the software's database and as previously reported in the literature, confirming the absence of oxidation. Aluminium had peaks at 2θ values of 38.6°, 44.8°, 65.2° and 78.3° [63,64], and copper had peaks at 43.3°, 50.4° and 74.1° [63,65].

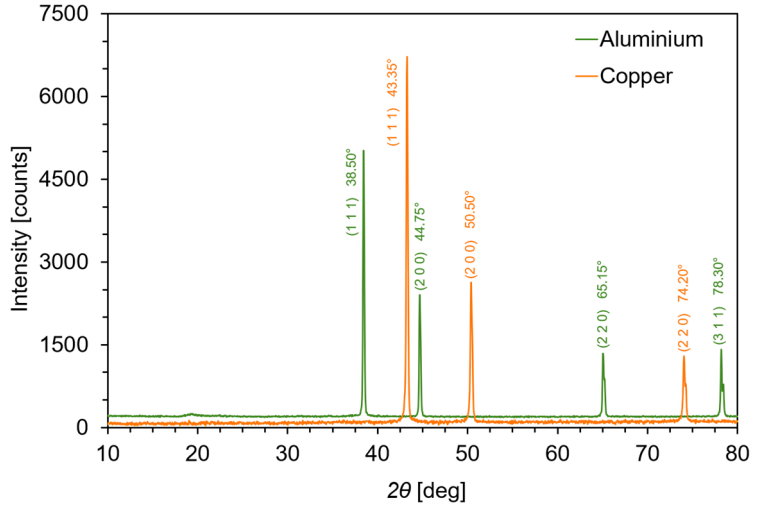

Figure 2. X-ray diffraction patterns of the metallic powders.

3.2. Mechanical Properties

Representative stress–strain tensile curves of the neat polymer and the produced composites are shown in Figure 3, and the obtained mechanical properties are presented in Table 4. In Figure 3, it is possible to observe that neat ABS presented the typical thermoplastic's stress–strain curve, with an elastic region, a prominent yield point and ductile break at greater strains [13]. Three out of four composites presented brittle behaviour. The tensile results indicate that the polymer/metal weight ratio has a significant effect on Young's modulus (E), tensile strength (σ_{max}), stress at break (σ_B) and strain at break (ε_B), and that there is a significant interaction between the weight ratio and type of filler (ANOVA, $p < 0.01$).

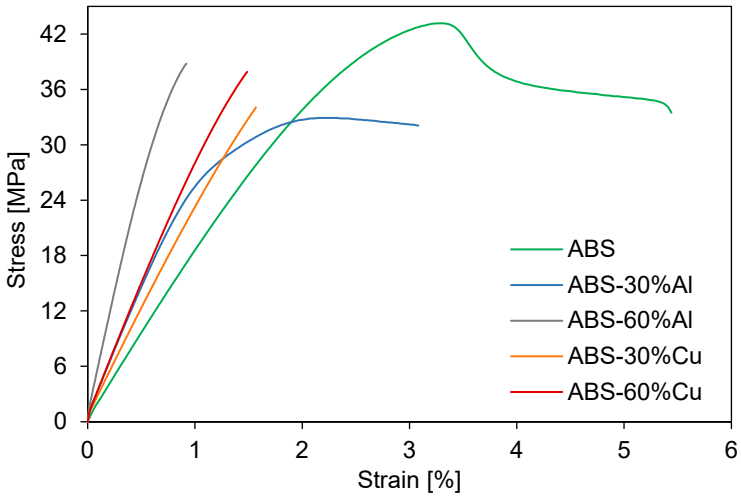

Figure 3. Representative stress–strain tensile curves of ABS and composites.

Table 4. Mechanical performance of injection-moulded ABS composites and respective standard deviations.

	ABS	**ABS-30%Al**	**ABS-60%Al**	**ABS-30%Cu**	**ABS-60%Cu**
Young's Modulus (E) [MPa]	1885.0 ±18.97	2837.5 ^{A} ±227.84	4784.4 ±47.04	2329.4 ±16.52	2853.1 ^{A} ±18.52
Yield Strength (σ_Y) [MPa]	43.4 ±0.36	32.4 ±0.54	- -	- -	- -
Strain at Yield (ε_Y) [%]	3.3 ±0.04	2.3 ±0.07	- -	- -	- -
Tensile Strength (σ_{max}) [MPa]	43.4 ±0.36	32.4 ^{B} ±0.67	39.4 ^{C} ±2.36	33.7 ^{B} ±1.71	38.1 ^{C} ±1.56
Stress at Break (σ_B) [MPa]	31.9 ^{D} ±3.64	31.3 ^{D} ±1.08	39.4 ^{E} ±2.36	33.7 ^{D} ±1.71	38.1 ^{E} ±1.56
Strain at Break (ε_B) [%]	5.2 ±1.44	2.9 ±0.58	1.0 ^{F} ±0.12	1.6 ^{F} ±0.11	1.5 ^{F} ±0.09
Impact Strength (IS) [kJ·m^{-2}]	13.71 ±0.304	2.70 ±0.090	2.03 ±0.072	3.12 ±0.092	4.30 ±0.081
Impact Resistance (IR) [kJ·m^{-1}]	139.33 ±3.088	27.40 ±0.912	20.67 ±0.731	31.72 ±0.931	43.68 ±0.825
Shore D Hardness	78.1 ±0.78	79.4 ±0.98	83.3 ^{G} ±1.27	83.2 ^{G} ±0.66	84.1 ±0.69

Values of average and standard deviations for σ_Y and ε_Y of ABS-30%Al refer to 12 specimens, as 4 specimens out of 16 presented a brittle fracture. All specimens of ABS-60%Al, ABS-30%Cu and ABS-60%Cu presented a brittle fracture during tensile testing; thus, no values of σ_Y and ε_Y are recorded. ^{A,B,C,D,E,F,G} Means that share a letter have no statistical differences.

The incorporation of metallic particles changed the mechanical response of ABS. The metallic particles significantly raised E for ABS-30%Al and ABS-60%Cu, whose values are close due to the similar filler volume fraction, in comparison to neat ABS (ca. 50%, $p < 0.01$), and for ABS-60%Al (over 250%, $p < 0.01$). ABS exhibited a mean yield point at σ_Y = 43.3 MPa and ε_Y = 3.3%, while ABS-30%Al featured yielding at σ_Y = 32.4 MPa and ε_Y = 2.3% followed by a ductile break at σ_B = 31.3 MPa and ε_B = 2.9%. All copper-loaded specimens failed before yielding during the tensile test, as well as all specimens of ABS-60%Al and 4 specimens out of 16 of ABS-30%Al. This reveals a major embrittling effect of the metallic filler on the matrix, representing a considerable loss in terms of toughness.

Overall, the mechanical behaviour observed under tensile loading follows a trend of increasing E and reducing ε_B as the filler content increases, as also reported by previous studies [1,9,41,57,66]. Moreover, E displays a linear dependence (R^2 = 0.9881) upon the volume fraction of the filler, regardless of the filler's nature (Figure 4). Young's modulus is not subjected to particle–matrix interfacial adhesion effects because debonding is not yet observed for small loads or displacements, i.e., the range within which the modulus is measured [66]. However, Masood and Song (2004, 2005) [9,10] reported a dependency of E and σ_{max} upon the size and content of metallic fillers: the larger the particle size, the greater the tensile modulus and strength.

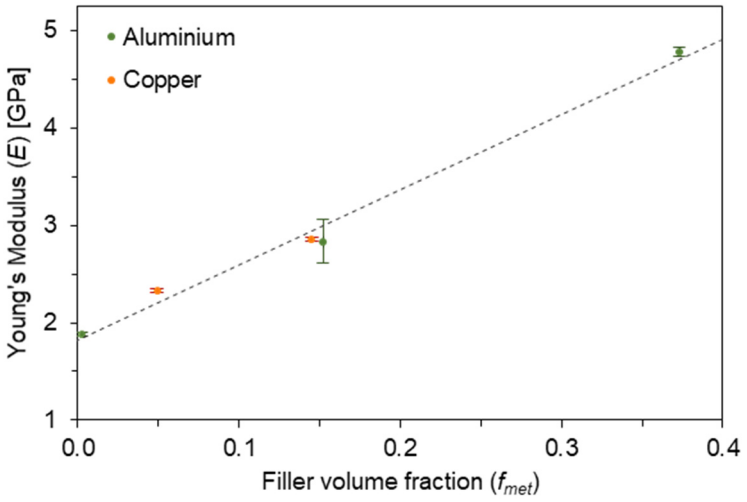

Figure 4. Young's modulus linear dependency upon reinforcement volume fraction.

Characteristics such as σ_{max} first decreased for a 30 wt% filler content and then, with a 60 wt% metal powder, increased to ca. 90% of that of neat ABS (Figure 5), while a significant increase of σ_B was observed for ABS-60%Al and ABS-60%Cu. Embrittlement, increase in E and decrease in ε_B are typically observed for ABS/aluminium composites [41,57]. In spite of the changes in injection moulding parameters due to the composites' increased viscosity, the injection pressure has minimal to low influence on the mechanical properties of injection-moulded ABS [67]. The most important parameter for E, σ_{max} and ε_B was identified as melt temperature, with impact levels weighting between 43 and 87%, whilst injection pressure made up between 2 to 22% for the same properties [67].

Although ABS-30%Al and ABS-60%Cu have similar filler volume fractions, σ_{max} and ε_B of such composites are significantly distinct ($p < 0.01$) and ABS-30%Al has ductile behaviour. This indicates that aluminium and copper promote distinct fracture mechanisms due to different levels of polymer–particle interface interactions. The polymer–metal interface is a crucial factor, and its integrity can be affected by the particle's morphology and stability, impairing the stress transfer between the matrix and the filler [13,66]. Since the formulations did not contain a coupling agent to promote enhanced interface interactions, there may be insufficient bonding between the metal particle and the polymer matrix [7].

ABS-30%Al and ABS-60%Cu have σ_{max} of 32.4 and 38.1 MPa, respectively, suggesting that the ABS–copper interface may be less weak than the ABS–aluminium one. As σ_{max} first drops for a 30 wt% filler content and then rises with 60 wt%, metal particles likely act as defects and have a weakening effect on ABS due to the stress concentration at a lower loading, later reinforcing the matrix as barriers to crack growth at higher concentrations [13,66]. Another reason for this may lie in the non-homogeneous dispersion of voids and particles, possibly leading agglomerations to cause stress concentrations [39].

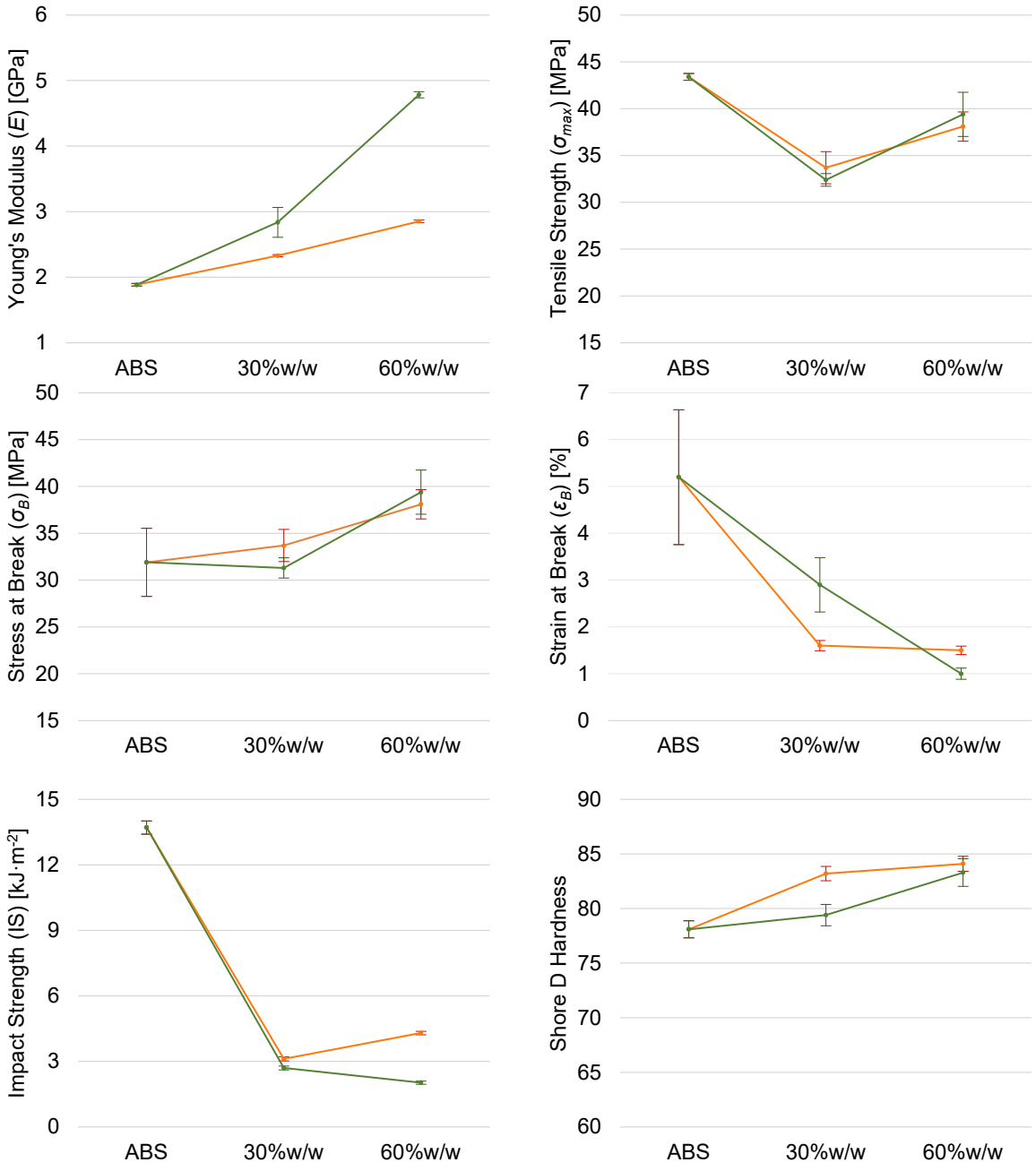

Figure 5. Interaction plots of selected mechanical properties of ABS/aluminium (green) and ABS/copper (orange) composites as functions of the metal powder content.

In ABS-30%Al, the poor interface bonding would cause ABS regions adjacent to the particle agglomerates to remain unaffected, withstanding a certain degree of plastic deformation. This is not observed for ABS-60%Al. The energy that can be absorbed by the ABS matrix is limited by the metal particles, leading to crack initiation and growth [68]. As the filler will not deform, it will rather debond; at the same time, the particles induce a concentration of tensile stress in the matrix, promoting multiple crazing sites [68].

The interaction between ABS and copper particles likely led the interface to stiffen neighbouring polymer segments from lower filler volume fractions, increasing the composite's brittleness. Increasing the filler concentration leads to the formation of clusters. Moreover, polymer–particle interfaces would act as breaking sites; therefore, as these agglomerations grow with the filler content, the surface-to-volume ratio drops, decreasing the amount of breaking sites, thus leading σ_B to rise [13].

The resulting brittleness observed in *E* is endorsed by a decrease in IS, with values for ABS-30%Al and ABS-60%Al as low as 20% and 15% of that of ABS, while ABS-30%Cu and ABS-60%Cu were as low as 23% and 31% relative to the pure material (Table 4 and Figure 5). The same trend was observed for IR. Such values of IS and IR suggest a poor adhesion between the matrix and reinforcement as a low-energy cleavage path leads to reduced energy absorption through the matrix [4,66,69]. In neat ABS, a fracture is driven by two simultaneous mechanisms, shear yielding and crazing, with shear-yielding bands acting as craze terminators and rigid particulates promoting enhanced shear yielding [68].

In general, the fracture toughness of ductile matrixes such as ABS is inversely proportional to the filler content due to a poor interfacial adhesion, particle agglomeration and non-homogeneous dispersion [66,70]. However, in spite of the reduction in toughness, the copper reinforcement particles likely promoted extra mechanisms for energy dissipation under a certain range of filler content, which is possibly associated with debonding and shear yielding, hence increasing the impact strength to some extent [66,68]. This would explain why increasing the copper content to 60 wt% enhanced the toughness behaviour as it raised IS by 38% relative to the 30 wt% copper content.

This effect was not observed for the aluminium composites as ABS-60%Al presented IS 25% lower than ABS-30%Al. In this case, the higher filler volume of aluminium reinforcement possibly led particles to agglomerate and act as stress concentration points, causing the impact properties to reduce, and supporting the hypothesis that the ABS–copper interface may be stronger than the ABS–aluminium one.

The cross-section fracture surfaces resulting from the Charpy test can be observed in Figure 6. ABS specimens presented clear evidence of deformation as the impact rupture took place, displaying the typical characteristics of a ductile rupture mechanism, including the presence of whitening due to the shear flow under stress [69]. These signals were absent on all the composites. Blisters can be observed on the composites cross-sections, likely caused by the moulding process, and could relate to the reduction in impact strength. Additionally, macroscopic aluminium agglomerations can be observed within the ABS matrix. Blisters observed on ABS-30%Cu were the largest overall. The amount and size of voids could also be related to the higher impact and tensile strength of ABS-60%Cu, as the non-homogeneous dispersion of blisters and particles might act as a point that creates stress concentrations. In Charpy impact testing, both the content and type of filler were found to be significant factors, and the interaction between the weight ratio and type of filler also had significant effects ($p < 0.01$). In addition, all the means were statistically different.

The values obtained for Shore D hardness showed an increasing trend alike to that of *E*, demonstrating that the stiffening effect due to the incorporation of the metal powders was also noticeable on the composites' surfaces. The highest hardness was recorded for ABS-60%Cu, a significant increase of 7.7% ($p < 0.01$) in comparison to neat ABS, which had the lowest hardness. The figures are similar to the results previously reported for ABS/aluminium composites [37,41].

Also, the decrease in impact strength due to the incorporation of a filler was found to take place in conjunction with an increase in hardness [69]. It has been suggested that the hard particle filler absorbs the load and withstands plastic deformation, thus resisting indentation [6]. In this context, the metallic particles would change the polymer matrix's microstructure; thus, the introduction of more grain boundaries due to increasing the metal content would cause the composite to reach a greater hardness value [71].

However, the lower values of hardness recorded for the aluminium-reinforced composites relative to the copper-filled ones, in spite of the greater volume fraction of the aluminium particles, may suggest an inadequate dispersion of the filler and a poorer interface effectiveness between the ABS matrix and aluminium reinforcement. Statistical analysis of the data indicates that both the content and type of filler have significant effects on the surface hardness characteristics, and the interaction between the weight ratio and type of filler was also found to be a significant factor (ANOVA, $p < 0.01$). In addition, only ABS-60%Al and ABS-30%Cu displayed no significant differences ($p = 0.988$).

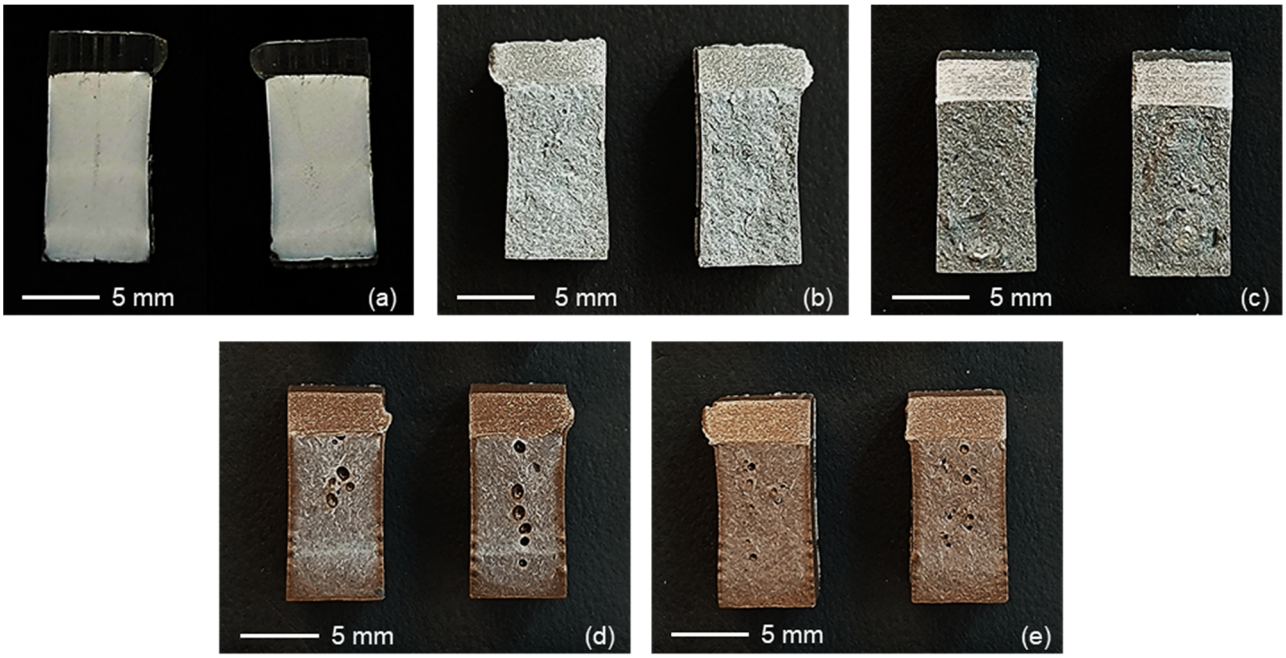

Figure 6. Representative fractographies from the Charpy impact test for (**a**) ABS, (**b**) ABS-30%Al, (**c**) ABS-60%Al, (**d**) ABS-30%Cu and (**e**) ABS-60%Cu; notches can be observed on the top of each cross-section.

3.3. Rheological Behaviour

The complex viscosity (η^*) mean values recorded at 195 °C for neat ABS and the metal-reinforced composites are presented in Figure 7 as a function of frequency (ω). There is a decrease of η^* with increasing ω, representing the shear thinning behaviour of ABS and the composites. The addition of metallic fillers did not change the overall η^* curve profile. Aluminium particles increased viscosity over the entire frequency range, while copper particles had a contrasting effect: ABS-30%Cu presented lower viscosity than ABS, indicating a possible plasticising effect due to the low volume fraction of Cu particles in the matrix, and ABS-60%Cu had a behaviour very close to that of neat ABS. Small amounts of a filler may reduce the viscosity as filler–filler interactions in the agglomerates would be weak and break under the shear force that orientates the flow direction [38]. At higher ω, the rate of decrease of η^* is greater, which is associated with the filler being forced to orient due to the shear stresses [51].

ABS presented a shear thinning parameter n of 0.4206. The changes in n for the composites are not large, with values ranging from 0.3962 for ABS-30%Cu to 0.4496 for ABS-60%Al, indicating low influence of the particles' dispersion on the rheological properties of ABS, which thus suggests low compatibility between the filler and polymer. In general, when there is a good interaction between the matrix and reinforcement, the slope of the η^* curve tends to increase, improving the shear thinning effect [52–56].

The increase in η^* of the ABS/aluminium composites accounts for the higher values of injection and holding pressure during the processing stage. Regarding the ABS/copper composites, despite a distinct trend of η^*, in order to achieve suitable moulding conditions those parameters were adjusted, preventing the polymer melt from freezing prematurely and to keep the mould pressurised.

The dependence of melt storage modulus (G') on ω is shown in Figure 8. The shoulder observed between 0.2 and 20 Hz can be attributed to the relaxation process of the butadiene domains within the styrene–acrylonitrile (SAN) phase. This typically represents the immiscibility of distinct phases of polymer blends and copolymers with discrete-continuous morphology [42]. The materials have nonterminal behaviour at both ends of the frequency

range, which means that the long-range motion of backbone chains is hindered during flow [54].

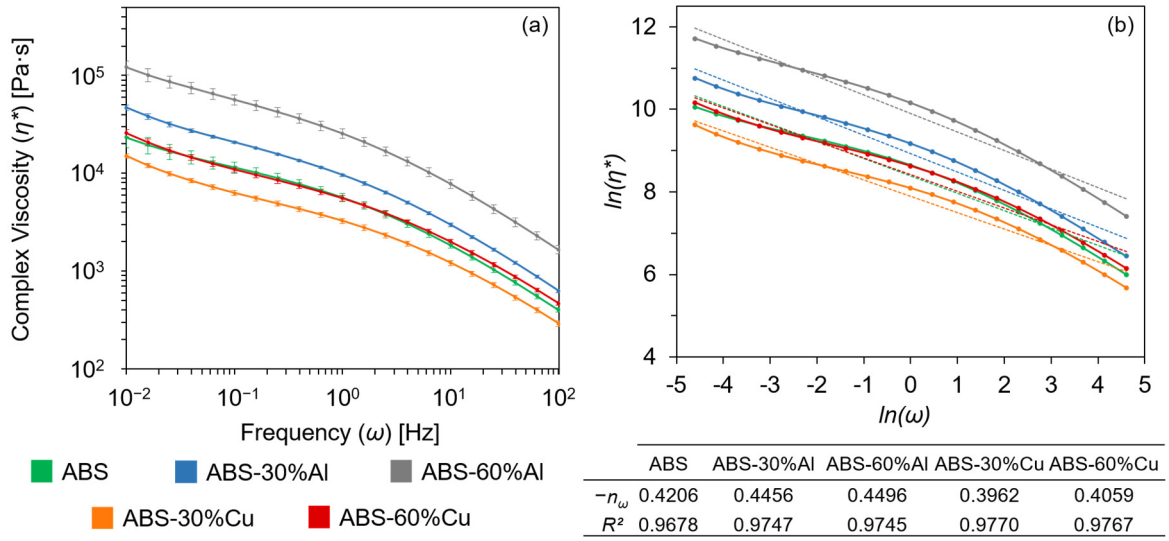

	ABS	ABS-30%Al	ABS-60%Al	ABS-30%Cu	ABS-60%Cu
$-n_\omega$	0.4206	0.4456	0.4496	0.3962	0.4059
R^2	0.9678	0.9747	0.9745	0.9770	0.9767

Figure 7. (**a**) The curves of η^* as a function of oscillation frequency; (**b**) the power law linear model for η^*, and the values of shear thinning parameter obtained from the linearisation of η^*.

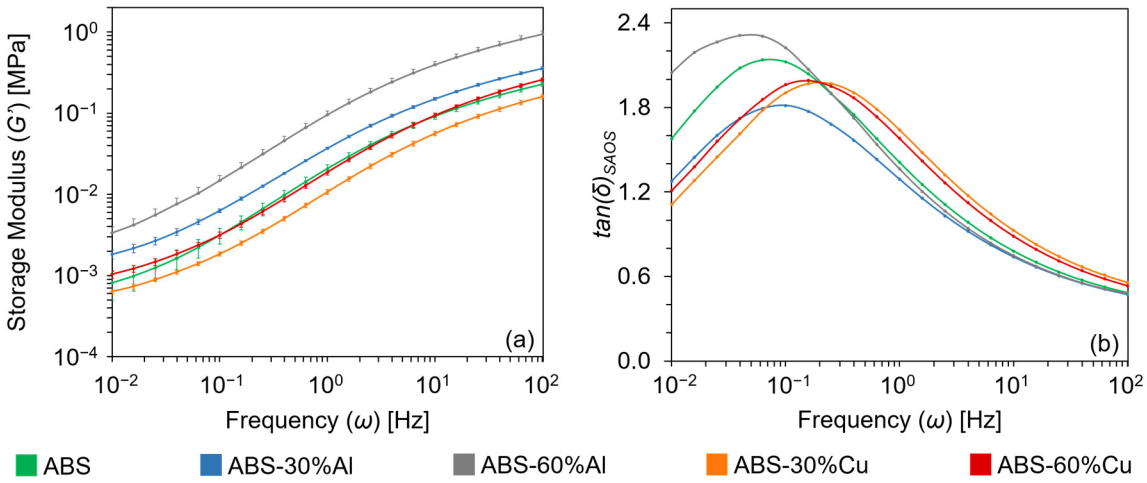

Figure 8. Curves of (**a**) melt storage modulus G' and (**b**) melt loss tangent $tan(\delta)_{SAOS}$ as functions of the oscillation frequency.

The change in G' at a given ω due to the type and content of reinforcement follows the same trend of change observed for η^*. Modulus shifts are observed on the ordinate axis, with minimal variations in the curve behaviour and no changes in the curve slope nor plateau developing at low ω. In composites with good matrix–filler interactions, G' rises with the filler content and develops a distinct plateau at low ω, which represents hindered chain relaxation due to the inability of filler particles to freely rotate [51,54,55]. ABS-60%Al displayed G' values ca. four times greater than those of ABS at all frequencies. The difference of G' between ABS and ABS-30%Al is greater at lower ω than at the higher end of the range, owing to a greater time to untangle chain entanglements at the lower end, but not enough time for chains to relax at higher ω [53]. Moreover, G' was found to overcome the loss modulus at higher ω, suggesting a viscous-to-elastic transition taking place [55].

Reinforcing a polymer matrix tends to reduce the melt $tan(\delta)_{SAOS}$ curve maxima, meaning a more elastic-like behaviour [52–54,56]. In this case, $tan(\delta)_{SAOS}$ decreased with

the incorporation of a filler due to hindrance in chain motion and relaxation during flow, as noticed for ABS-30%Al, ABS-30%Cu and ABS-60%Cu relative to ABS, with their maxima shifting to higher ω. All samples displayed a slope transition within the low-frequency range, which may be associated with the hindered mobility of polymer chains, formation of three-dimensional network structures of fillers or a change in the filler–matrix interface interaction [53]. This greatly contrasts with the data regarding η^* and G', whose maximum values were achieved with ABS-60%Al. The lack of consistency of such results might further reveal that the affinity between the ABS matrix and the metallic reinforcement is poor.

Since MFB is a crucial parameter for 3D printing, SAOS has been employed to determine the appropriate processing conditions for high-performance thermoplastic AM feedstock, such as ABS. Ajinjeru et al. (2018) [56] assessed the effects of temperature, reinforcement and angular frequency on η^* of ABS and ABS/carbon fibre (ABS/CF) composites. It was reported that η^* reduced with the increase in the processing temperature from 230 to 270 °C and increase in ω, but was boosted with the incorporation of carbon fibres, enhancing the shear thinning effect. Finally, the authors claimed that the AM system's deposition temperature may have a significant impact on η^*, which is crucial when selecting the screw speed of large fabrication AM (LFAM) processes [56]. The increase in viscosity causes the torque on the extrusion screw to rise as well, so that the screw load excess may perform a counterbalancing action by adjusting the temperature, enabling a wide processing window by adjusting the flow rate [56]. Moreover, higher mixing screw speeds reportedly impart increased melting shear, thus significantly enhancing the filler dispersion, which in turn improves the composites' mechanical and thermal properties [72]. Regarding the processing temperature limits, ABS presents a main degradation step that starts from 300 °C, with an onset point at ca. 365 °C; therefore, no thermal degradation events are expected to take place within the temperature range utilised in the test [73,74].

3.4. Viscoelastic Properties

The storage modulus (E') mean values recorded at 30 and 90 °C, the glass transition temperature (T_g) of neat ABS and the metal-reinforced composites are presented in Table 5. Representative dynamic mechanical response curves of E' and the damping factor ($tan(\delta)_{DMA}$) as functions of temperature are displayed in Figure 9.

Table 5. Dynamic mechanical responses of ABS and its composites.

	ABS	ABS-30%Al	ABS-60%Al	ABS-30%Cu	ABS-60%Cu
E' (30 °C) [MPa]	2064.5 ±40.7	2878.0 ±190.7	4444.3 ±206.6	2636.3 ±164.7	3259.3 ±153.1
E' (90 °C) [MPa]	1097.8 ±41.2	1820.0 ±49.1	3201.3 ±178.1	1155.7 ±30.2	1666.0 ±42.9
T_g [°C]	110.0 ±0.61	114.1 ±1.50	117.8 ±1.82	107.0 ±0.21	109.7 ±0.52

For the neat ABS matrix, E' curve shows the glassy state plateau from 25 to 80 °C and the glass transition from 80 °C onwards. Copper-filled composites closely followed the same behaviour. On the other hand, aluminium-reinforced composites had the glass transition shifted by ca. 5 °C, with the glassy state plateau prevailing up to 85 °C and shifting the end of the glass transition to higher temperatures as well. At 30 °C, all the composites have E' values greater than that of the pure matrix, with the lowest being 28% higher at 2636.3 MPa for ABS-30%Cu, and the highest being 115% greater at 4444.3 MPa for ABS-60%Al.

In addition, E' was also found to have a linear dependence (R^2 = 0.9881) upon the volume fraction of the filler at 30 °C, mirroring the similar trend observed for Young's modulus. When analysing ABS and ABS/Al composites only, such linear dependence achieves R^2 = 0.9972, whereas ABS/Cu composites have a positive deviation respective

to the linear regression model. Comparing ABS-30%Al and ABS-60%Cu, which have similar reinforcement volume fractions, it is noticed that the latter exhibits higher E'. These observations endorse the hypothesis of a better interface bonding between ABS and copper powder than between ABS and aluminium powder [75].

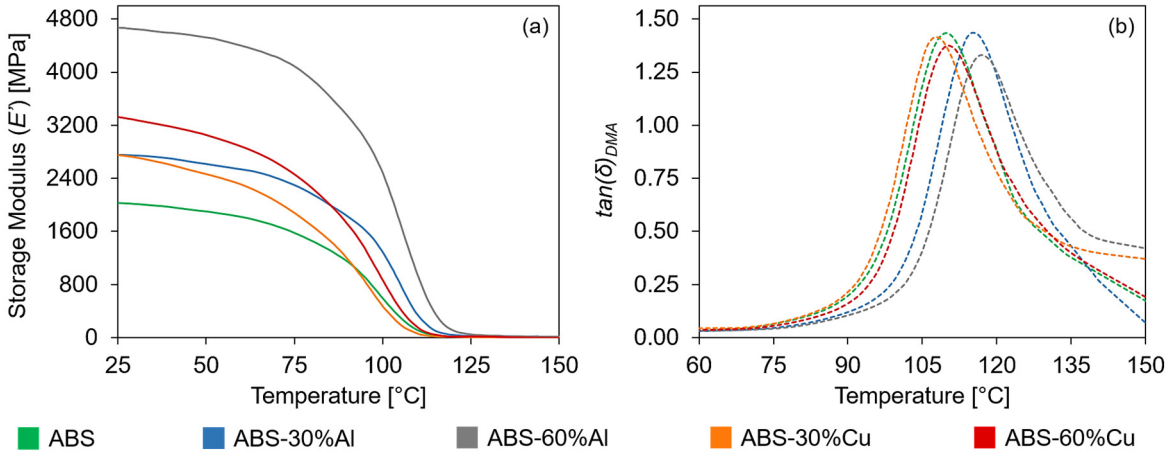

Figure 9. Effect of the metallic fillers on (**a**) storage modulus E' and (**b**) damping factor $tan(\delta)_{DMA}$ of ABS.

Overall, the composites' storage moduli are greater than that of ABS within the whole range of the glassy plateau, revealing that the metal reinforcement particles have a stiffening effect on the matrix, i.e., the metallic powders had a strong interlocking action in the ABS matrix, increasing the material's stiffness [7,55,74]. This effect is more pronounced for ABS/Al composites than for ABS/Cu, as the glassy state plateau lasts longer and the E' curves of ABS-30%Cu and ABS-60%Cu are overcome by ABS and ABS-30%Al, respectively, during the glass transition. At 90 °C, the temperature effects are evident as ABS-30%Cu displayed E' only 5% higher than ABS, and ABS-60%Cu had its E' reduced to 8.5% lower than that of ABS-30%Al. A possible reason for this would be a loss of effectiveness of the ABS/Cu interface due to increasing temperature [75].

The metal powders also affected the glass transition of the SAN phase of ABS, as shown in Table 5 and Figure 9. It is known that the T_g of ABS is at approximately 100 °C and relates to the glassy–rubbery transition of the SAN grafting block [25,33,39,57]. The maxima of the $tan(\delta)_{DMA}$ curves obtained with DMA displayed the same trend of change in ascending order as exhibited by G' and η^*.

Aluminium particles hindered the motion and rotation of ABS chains and retarded the onset of the viscous component contribution, as was observed with the increase in G', raising the T_g up to 117.8 °C for ABS-60%Al. The reinforcement introduces restrictions on the segmental mobility of interfacial SAN blocks, tending to increase the T_g due to mechanical locking [33,74]. Composites containing a 60 wt% filler have greater T_g than 30 wt% composites, owing to the confinement of the polymer within the filler particles and the consequential clamping effect [13]. An increase in the reinforcement particle size would also increase the T_g for the same loading levels [57].

ABS-30%Cu had the lowest T_g at 107.0 °C, which is a clear drop relative to 110.0 °C of ABS. This suggests that, at that filler volume fraction and with that particle size, the Cu powder had some plasticising effect into the SAN phase blocks by likely disrupting and weakening the intermolecular interactions between polymer chains, possibly due to a better dispersion of the smaller particles, likely combined with a probable loss of intensity in the polymer–metal interface bonding due to an increased free volume when the temperature was increased. This also relates to the reduction in η^* and G' observed for ABS-30%Al.

Increasing the copper content to 60 wt% T_g rose to 109.7 °C, representing a recovery of interlocking. As the T_g of ABS-60%Cu is close to that of ABS and lower than ABS-30%Al,

the reinforcement loading is not the only factor affecting the glass transition, supporting the hypothesis that the ABS-copper particles' surface interactions display an adverse response brought about by temperature elevation. Therefore, despite the possible loss of the ABS-Cu interface's effectiveness with temperature, the size difference between aluminium and copper particles is likely related to the distinct T_g values recorded for ABS-30%Al and ABS-60%Cu.

3.5. Thermal Properties

Thermal conductivity results are shown in Figure 10. ABS has the lowest k at 0.460 $W \cdot K^{-1} \cdot m^{-1}$, while ABS-60%Al has the highest at 0.861 $W \cdot K^{-1} \cdot m^{-1}$, which is a significant increase of 87% ($p < 0.01$). For thermal conductivity, the filler volume fraction arises as a crucial factor since studies suggest that, beyond a minimum filling threshold, particle agglomerates would create a conductive path owing to the increased contact area, enhancing thermal conduction properties [4,6,7,71]. Increasing the filling content would reduce the space between reinforcement particles, hence increasing the probability of effective contact between neighbouring particles to form a conductive path [7].

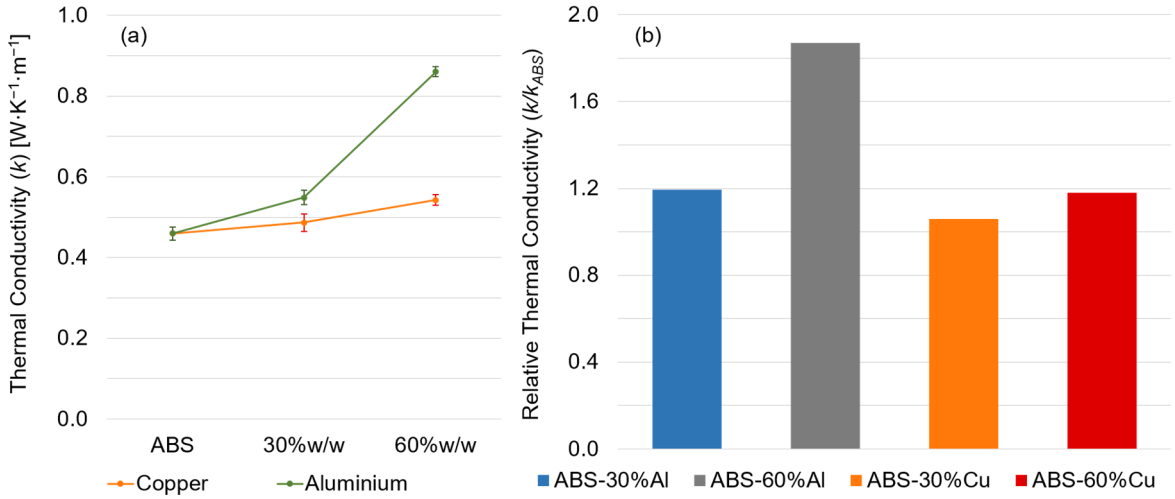

Figure 10. (**a**) Interaction plot of thermal conductivity of ABS and composites as a function of weight ratio; (**b**) relative thermal conductivity of the composites.

The results obtained by Masood and Song (2004, 2005) [9,10] suggested that the composites' thermal conductivity rose with the size and volume content of metal particles. This would indicate that copper powder at 30 wt% loading is insufficient to produce a conductive path within the polymeric matrix, and this also clarifies why ABS-30%Al and ABS-60%Cu have close values of k. In addition, the conductive path also depends upon the size of the reinforcement particles and the dispersion of voids, blisters and particle agglomerates [71]. Nikzad et al. (2011) [7] reported that volume fractions of copper particles lower than 0.10 cannot break the thermal resistance of the ABS matrix; thus, the threshold point of f_{met} would have to be between 0.1 and 0.2.

Contrastingly, an increase of 41% in the thermal conductivity of ABS loaded with 50 wt% Cu relative to the neat material has been described [1]. Values of k for ABS have been reported as 0.646 $W \cdot K^{-1} \cdot m^{-1}$ [1], 0.17 $W \cdot K^{-1} \cdot m^{-1}$ [4] and 0.145 $W \cdot K^{-1} \cdot m^{-1}$ [6]. Such differences could be explained by the distinct specimen manufacturing techniques and measurement methods in each study. In injection-moulded particulate-reinforced composites, the moulding process is believed to align the filler in the melt flow direction, and both the contact area and orientation are promoted due to the high injection pressures; thus, heat and charge transport is expected to be superior to that seen in 3D-printed parts [4]. This also could help explain the higher thermal conductivity obtained for ABS/Al composites in spite of copper's well-known greater conductivity properties, as processing

parameters such as the injection pressure had to be adjusted and accounted for the higher melt viscosity. Moreover, in general, the thermal conductivity of polymer composites depends upon various factors, e.g., filler content, filler shape and size, interfacial adhesion, resistance of the filler–polymer interface and filler structure quality within the matrix [76].

In addition, k demonstrated a linear dependence (R^2 = 0.9465) upon the volume fraction of the filler, following similar trends found for Young's and storage moduli, endorsing the results obtained by Masood and Song (2005) [10]. When analysing ABS and ABS/Cu composites only, the linear regression model yields R^2 = 0.9999. There are no significant statistical differences between ABS and ABS-30%Cu (0.027 $W \cdot K^{-1} \cdot m^{-1}$, p = 0.263), or between ABS-30%Al and ABS-60%Cu (0.006 $W \cdot K^{-1} \cdot m^{-1}$, p = 0.985). In addition, results indicate that both the content and type of filler have significant effects on k, and the interaction between the type of filler and weight ratio was also found to be a significant factor (ANOVA, $p < 0.01$).

3.6. Morphological Characterisation of the Composites

The SEM fractographies of the cross-section fracture surfaces resulting from the Charpy impact test are shown in Figure 11**,** allowing an assessment of the dispersion and agglomeration of the two metal powders within the ABS matrix. Aluminium particles were observed to be larger than copper particles. Moreover, the size of the aluminium particles in the composites seems bigger than when first introduced in the mixture at the processing stage. This suggests that this metal has a stronger filler–filler interaction, allowing a greater mobility in the molten matrix during the processing stages and a trend to aggregate, forming non-homogeneously dispersed agglomerations.

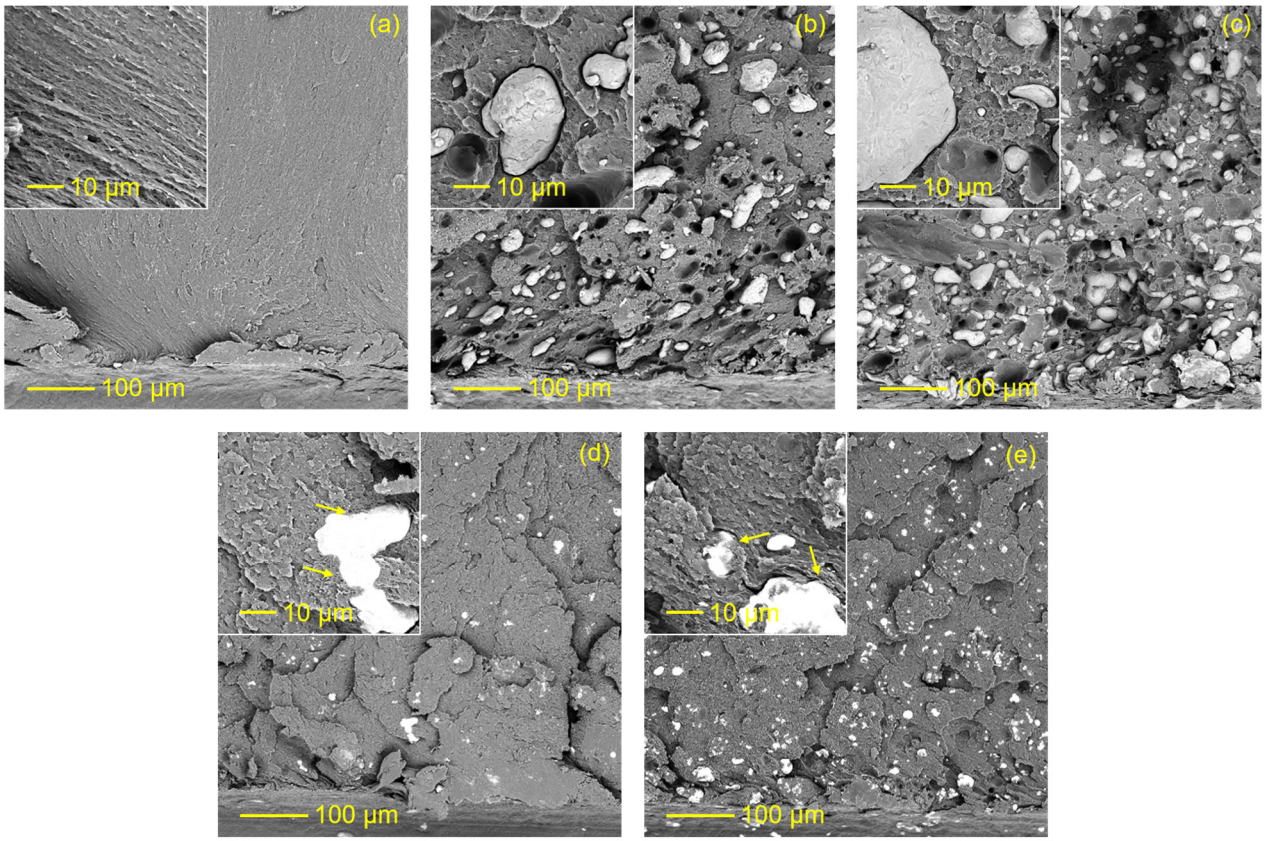

Figure 11. Representative SEM fractographies: (**a**) ABS, (**b**) ABS-30%Al, (**c**) ABS-60%Al, (**d**) ABS-30%Cu and (**e**) ABS-60%Cu. Notches can be observed on the bottom of each cross-section. Arrows indicate regions of matrix–particle adherence with bridging in ABS/Cu composites.

The quality of metal particle dispersion can also be verified through an elemental analysis that unveils the chemical composition of a surface through EDS mapping, as shown in Figure 12. Comparing ABS-30%Al and ABS-60%Cu and considering their comparable filler volume fraction f_{met}, the copper particles appear to manifest a better dispersion than aluminium particles. This supports the hypothesis of a better interaction of ABS with copper rather than with aluminium, resulting in a more effective polymer–filler interface. At lower filler contents, the composites contain a higher proportion of the ABS matrix compared to reinforcements. This hinders the contact between the metal particles in ABS, endorsing the dependency of thermal conductivity upon the content and volume ratio of the filler.

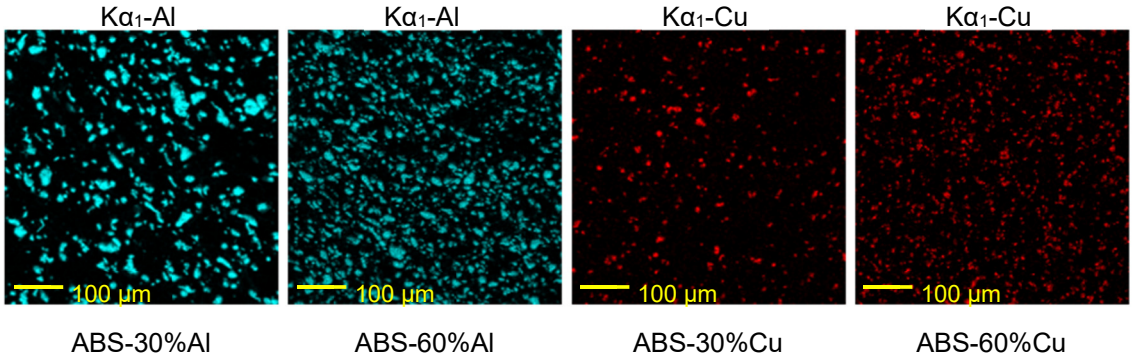

Figure 12. Dispersion of aluminium and copper particles within the composites' matrix obtained with EDS surface chemical composition mapping.

When undergoing a high strain rate test such as the impact one, polymer chains are subjected to extreme stresses until they undergo rupture, leading to the nucleation of microvoids in the matrix. SEM imaging enabled a further insight into the impact fracture surfaces (Figure 11), supporting the observations based on Figure 6 since indications of a plastic deformation during an impact rupture are once again clearly seen for neat ABS but not for the composites [69,74]. The occurrence of fibrils further endorses the extent of the plastic deformation in ABS, as the growth and propagation of the macroscopic crack (notch) is thought to be accompanied by the formation of additional plastic microcracks [74]. The SEM fractographies show clear differences between the aluminium- and copper-reinforced composites (Figure 11). The lack of bonding between the ABS matrix and aluminium particles becomes evident as there are considerable gaps (debonding) surrounding the Al filler. Moreover, hollow spaces (cupules), previously occupied by particles that were pulled out during the impact test, are visible. On the other hand, Cu particles display less debonding but are embedded in the ABS matrix, which is evinced by polymer segments attached to filler particles, instead of signs of pull-out as a result of the impact test. However, both composites present a layered structure comprising small aligned steps on the fracture surface, which indicates shear yielding [77].

Additionally, aluminium and copper composites presented distinct distributions of microvoids and crazes along the matrix. In the case of ABS/Al composites, cracks were initiated from microvoids on the weak matrix–filler interface and they coalesced towards the neighbouring particles, resulting in failure propagation through reinforcement debonding and pull-out and the formation of cupules [74,77,78]. On the other hand, in the case of ABS/Cu composites, metal particles plastically bridged the crazes due to their adherence to the matrix, preventing them from spreading and becoming cracks and favouring the nucleation of microvoids [77,79,80]. These effects are likely due to the different nature of each reinforcement as well as their particular characteristics and may have a significant impact on the mechanical properties of the composite, as its failure mode is affected by the wettability of the filler by the matrix [81,82]. In this sense, according to Ryder et al. (2018) [83], water-atomised metal particles, such as the copper ones in this study, are non-

spherical, morphologically irregular and rough, which improves interfacial interactions between reinforcement particles and the polymer matrix.

4. Conclusions

Metal-reinforced thermoplastic composites are suitable materials for applications requiring special thermal, electrical or magnetic properties, enabling one to benefit from properties that usual polymer materials lack. Making these composites into filament wires for feedstock could potentially lead to high-performance, functional prototypes for a wide range of applications that could be manufactured with additive manufacturing (AM) processes, which would enable these materials to be quickly shaped into any design. Dynamic rheology is crucial to determine the appropriate processing conditions for AM feedstock as melt flow behaviour (MFB) is an important parameter for 3D printing. ABS composites reinforced with aluminium and copper particles were produced and injection-moulded and then characterised regarding their mechanical, rheological, viscoelastic and thermal properties.

Tensile testing revealed that the Young's modulus increased with the metal particle incorporation and followed the law of mixtures, displaying a linear dependence upon the filler volume fraction. However, there was an embrittling effect, evinced by the lower elongation at break and impact strength owing to a poor matrix–filler interface unable to properly transfer load.

Small angle oscillatory shear (SAOS) supported the low affinity between ABS and the metallic fillers as the complex viscosity (η^*) did not exhibit an enhancement of the shear thinning effect, with Al particles causing η^* to rise. DMA results unveiled that changes in viscoelastic properties are mainly due to the mechanical locking of backbone chains by filler particles.

Below T_g, ABS/Cu composites behave similarly to ABS/Al; however, as they undergo the glass transition, the copper filler acts as a plasticising agent, with composites featuring characteristics closer to those presented by neat ABS both in SAOS and DMA.

Thermal conductivity (k) was improved with the incorporation of the metals, especially aluminium, due to its lower density relative to copper, indicating that k also follows the law of mixtures and depends on the filler volume fraction. SEM imaging confirmed the poor interaction between the ABS matrix and aluminium and copper fillers (as debonding and pull-out were observed) and disclosed that the metals were associated with different fracture mechanisms.

Overall, the attained set of mechanical, rheological and viscoelastic properties offers a promising opportunity to optimise the processing–property relationship in spite of the poor matrix–filler interface, which can be improved using higher mixing speeds, considering the wide processing window available. Therefore, the obtained materials are potential candidates for metal-reinforced thermoplastic composites that could be processed through AM technologies.

Author Contributions: Conceptualisation, V.F.M., C.A.F. and D.M.D.; methodology, V.F.M.; validation, V.F.M. and H.P.; formal analysis, V.F.M. and H.P.; investigation, V.F.M. and H.P.; data curation, V.F.M.; writing—original draft preparation, V.F.M. and H.P.; writing—review and editing, V.F.M.; visualisation, V.F.M.; supervision, J.S.C., C.A.F. and D.M.D.; project administration, C.A.F. and D.M.D.; funding acquisition, D.M.D. All authors have read and agreed to the published version of the manuscript.

Funding: This publication contains results from research conducted with the financial support of Enterprise Ireland under the Technology Gateway Programme, grant number TG-2017-0114 (APT Ireland), and the Science Foundation Ireland (SFI), grant number SFI 16/RC/3918, co-funded by the European Regional Development Fund.

Data Availability Statement: All the data necessary to reproduce the results and support the conclusions are included within this paper. Further details may be provided upon request.

Acknowledgments: The authors would like to thank the APT Ireland staff, for assisting with the extrusion and injection moulding processes; Annelise Alves (UFRGS), for the BET analyses; Eduardo G. Barboza (UFRGS), for the granulometry tests; Lucas B. Gomes (UFRGS), for the XRD analyses; and Rodrigo A. Barbieri (UCS), for assisting with SEM/EDS analyses. The authors would also like to thank the funding agencies Enterprise Ireland, Science Foundation Ireland (SFI), Higher Education Authority (HEA), The Department of Further and Higher Education, Research, Innovation and Science (D/FHERIS), National Council for Scientific and Technological Development (CNPq) and CAPES Foundation for financial support.

Conflicts of Interest: The authors declare no conflict of interest.

References

1. Hwang, S.; Reyes, E.I.; Moon, K.; Rumpf, R.C.; Kim, N.S. Thermo-mechanical Characterization of Metal/Polymer Composite Filaments and Printing Parameter Study for Fused Deposition Modeling in the 3D Printing Process. *J. Electron. Mater.* **2015**, *44*, 771–777. [CrossRef]
2. Kalsoom, U.; Peristyy, A.; Nesterenko, P.N.; Paull, B. A 3D printable diamond polymer composite: A novel material for fabrication of low cost thermally conducting devices. *RSC Adv.* **2016**, *6*, 38140–38147. [CrossRef]
3. Carson, J.K.; Alsowailem, M. Thermal Diffusivity of Copper/Linear-low-density Polyethylene Composites. *Polym. Polym. Compos.* **2017**, *25*, 447–452. [CrossRef]
4. Quill, T.J.; Smith, M.K.; Zhou, T.; Baioumy, M.G.S.; Berenguer, J.P.; Cola, B.A.; Kalaitzidou, K.; Bougher, T.L. Thermal and mechanical properties of 3D printed boron nitride—ABS composites. *Appl. Compos. Mater.* **2018**, *25*, 1205–1217. [CrossRef]
5. Palmero, E.M.; Casaleiz, D.; de Vicente, J.; Hernández-Vicen, J.; López-Vidal, S.; Ramiro, E.; Bollero, A. Composites based on metallic particles and tuned filling factor for 3D-printing by Fused Deposition Modeling. *Compos. Part A Appl. Sci. Manuf.* **2019**, *124*, 105497. [CrossRef]
6. Hamzah, K.A.; Yeoh, C.K.; Noor, M.M.; Teh, P.L.; Aw, Y.Y.; Sazali, S.A.; Wan Ibrahim, W.M.A. Mechanical properties and thermal and electrical conductivity of 3D printed ABS-copper ferrite composites via 3D printing technique. *J. Thermoplast. Compos. Mater.* **2022**, *35*, 3–16. [CrossRef]
7. Nikzad, M.; Masood, S.H.; Sbarski, I. Thermo-mechanical properties of a highly filled polymeric composites for Fused Deposition Modeling. *Mater. Des.* **2011**, *32*, 3448–3456. [CrossRef]
8. Yu, J.H.; Cennini, G. Improving thermal conductivity of polymer composites in embedded LEDs systems. *Microelectron. J.* **2014**, *45*, 1829–1833. [CrossRef]
9. Masood, S.H.; Song, W.Q. Development of new metal/polymer materials for rapid tooling using Fused deposition modelling. *Mater. Des.* **2004**, *25*, 587–594. [CrossRef]
10. Masood, S.H.; Song, W.Q. Thermal characteristics of a new metal/polymer material for FDM rapid prototyping process. *Assem. Autom.* **2005**, *25*, 309–315. [CrossRef]
11. Moritz, V.F.; Bezerra, G.S.N.; Hopkins Jnr, M.; Fuenmayor, E.; Günbay, S.; Hayes, C.; Lyons, J.G.; Devine, D.M. Heat Dissipation Plays Critical Role for Longevity of Polymer-Based 3D-Printed Inserts for Plastics Injection Moulding. *J. Manuf. Mater. Process.* **2022**, *6*, 117. [CrossRef]
12. Coser, E.; Moritz, V.F.; Krenzinger, A.; Ferreira, C.A. Development of paints with infrared radiation reflective properties. *Polímeros* **2015**, *25*, 305–310. [CrossRef]
13. Merazzo, K.J.; Díez, A.G.; Tubio, C.R.; Manchado, J.C.; Malet, R.; Pérez, M.; Costa, P.; Lanceros-Mendez, S. Acrylonitrile Butadiene Styrene-Based Composites with Permalloy with Tailored Magnetic Response. *Polymers* **2023**, *15*, 626. [CrossRef] [PubMed]
14. Sofian, N.M.; Rusu, M.; Neagu, R.; Neagu, E. Metal Powder-Filled Polyethylene Composites. V. Thermal Properties. *J. Thermoplast. Compos. Mater.* **2001**, *14*, 20–33. [CrossRef]
15. Mamunya, Y.P.; Davydenko, V.V.; Pissis, P.; Lebedev, E.V. Electrical and thermal conductivity of polymers filled with metal powders. *Eur. Polym. J.* **2002**, *38*, 1887–1897. [CrossRef]
16. Luyt, A.S.; Molefi, J.A.; Krump, H. Thermal, mechanical and electrical properties of copper powder filled low-density and linear low-density polyethylene composites. *Polym. Degrad. Stab.* **2006**, *91*, 1629–1636. [CrossRef]
17. Tekce, H.S.; Kumlutas, D.; Tavman, I.H. Effect of Particle Shape on Thermal Conductivity of Copper Reinforced Polymer Composites. *J. Reinf. Plast. Compos.* **2007**, *26*, 113–121. [CrossRef]
18. Chifor, V.; Orban, R.L.; Tekiner, Z.; Turker, M. Thermal, Mechanical and Electrical Properties of High Density Polyethylene Composites Reinforced with Copper Powder. *Mater. Sci. Forum* **2011**, *672*, 191–194. [CrossRef]
19. Carson, J.K.; Noureldin, M. Measurements of the thermal diffusivity of linear-medium-density-polyethylene/aluminium composites using a transient comparative method. *Int. Commun. Heat Mass Transf.* **2009**, *36*, 458–461. [CrossRef]
20. Carson, J.K. Measurement and modelling of the thermal conductivity of dispersed aluminium composites. *Int. Commun. Heat Mass Transf.* **2011**, *38*, 1024–1028. [CrossRef]
21. Rahmati, S.; Dickens, P. Rapid tooling analysis of Stereolithography injection mould tooling. *Int. J. Mach. Tools Manuf.* **2007**, *47*, 740–747. [CrossRef]

22. Pontes, A.J.; Cousa, C.; Gomes, C.; Pouzada, A.S. Development of efficient composite systems for the production of resin cast moulding blocks. In *Proceedings of the PPS 24th Annual Meeting*; Polymer Processing Society: Salerno, Italy, 2008.
23. Ranjan, N.; Kumar, R.; Kumar, R.; Kaur, R.; Singh, S. Investigation of Fused Filament Fabrication-Based Manufacturing of ABS-Al Composite Structures: Prediction by Machine Learning and Optimization. *J. Mater. Eng. Perform.* **2023**, *32*, 4555–4574. [CrossRef]
24. Akrout, M.; Ben Difallah, B.; Kharrat, M.; Dammak, M.; Pereira, A.; Oliveira, F.J.; Duarte, I. On the Structural, Thermal, Micromechanical and Tribological Characterizations of Cu-Filled Acrylonitrile Butadiene Styrene Micro-Composites. *Materials* **2023**, *16*, 6428. [CrossRef] [PubMed]
25. Sa'ude, N.; Masood, S.H.; Nikzad, M.; Ibrahim, M.; Ibrahim, M.H.I. Dynamic mechanical properties of copper-ABS composites for FDM feedstock. *Int. J. Eng. Res. Appl.* **2013**, *3*, 1257–1263.
26. Dawoud, M.; Taha, I.; Ebeid, S.J. Mechanical behaviour of ABS: An experimental study using FDM and injection moulding techniques. *J. Manuf. Process.* **2016**, *21*, 39–45. [CrossRef]
27. Wang, X.; Jiang, M.; Zhou, Z.; Gou, J.; Hui, D. 3D printing of polymer matrix composites: A review and prospective. *Compos. Part B Eng.* **2017**, *110*, 442–458. [CrossRef]
28. Gong, K.; Liu, H.; Huang, C.; Cao, Z.; Fuenmayor, E.; Major, I. Hybrid Manufacturing of Acrylonitrile Butadiene Styrene (ABS) via the Combination of Material Extrusion Additive Manufacturing and Injection Molding. *Polymers* **2022**, *14*, 5093. [CrossRef]
29. Gong, K.; Xu, H.; Liu, H.; Cao, Z.; Fuenmayor, E.; Major, I. Hybrid manufacturing of mixed-material bilayer parts via injection molding and material extrusion three-dimensional printing. *J. Appl. Polym. Sci.* **2023**, *140*, e53972. [CrossRef]
30. Zhang, W.; Cotton, C.; Sun, J.; Heider, D.; Gu, B.; Sun, B.; Chou, T.-W. Interfacial bonding strength of short carbon fiber/acrylonitrile-butadiene-styrene composites fabricated by fused deposition modeling. *Compos. Part B Eng.* **2018**, *137*, 51–59. [CrossRef]
31. Sa'ude, N.; Ibrahim, M.; Ibrahim, M.H.I.; Wahab, M.S.; Haq, R.; Marwah, O.M.F.; Khirotdin, R.K. Additive manufacturing of copper-ABS filament by fused deposition modeling (FDM). *J. Mech. Eng.* **2018**, *5*, 23–32.
32. Abeykoon, C.; Sri-Amphorn, P.; Fernando, A. Optimization of fused deposition modeling parameters for improved PLA and ABS 3D printed structures. *Int. J. Light. Mater. Manuf.* **2020**, *3*, 284–297. [CrossRef]
33. Billah, K.M.M.; Lorenzana, F.A.R.; Martinez, N.L.; Wicker, R.B.; Espalin, D. Thermomechanical characterization of short carbon fiber and short glass fiber-reinforced ABS used in large format additive manufacturing. *Addit. Manuf.* **2020**, *35*, 101299. [CrossRef]
34. Akhoundi, B.; Modanloo, V. A multi-criteria decision-making analysis on the extrusion-based additive manufacturing of ABS/Cu composites. *Int. J. Interact. Des. Manuf.* **2023**, *17*, 1995–2003. [CrossRef]
35. Isa, N.M.A.; Sa'ude, N.; Ibrahim, M.; Hamid, S.M.; Kamarudin, K. A Study on Melt Flow Index on Copper-ABS for Fused Deposition Modeling (FDM) Feedstock. *Appl. Mech. Mater.* **2015**, *773–774*, 8–12. [CrossRef]
36. Sa'ude, N.; Ibrahim, M.; Ibrahim, M.H.I. Melt flow rate (MFR) of ABS-copper composite filament by fused deposition modeling (FDM). *ARPN J. Eng. Appl. Sci.* **2016**, *11*, 6562–6567.
37. Singh, R.; Kumar, R.; Ahuja, I. Mechanical, thermal and melt flow of aluminum-reinforced PA6/ABS blend feedstock filament for fused deposition modeling. *Rapid Prototyp. J.* **2018**, *24*, 1455–1468. [CrossRef]
38. Kumar, N.; Jain, P.K.; Tandon, P.; Pandey, P.M. Investigations on the melt flow behaviour of aluminium filled ABS polymer composite for the extrusion-based additive manufacturing process. *Int. J. Mater. Prod. Technol.* **2019**, *59*, 194. [CrossRef]
39. Alghadi, A.M.; Tirkes, S.; Tayfun, U. Mechanical, thermo-mechanical and morphological characterization of ABS based composites loaded with perlite mineral. *Mater. Res. Express* **2019**, *7*, 015301. [CrossRef]
40. Sezer, H.K.; Eren, O. FDM 3D printing of MWCNT re-inforced ABS nano-composite parts with enhanced mechanical and electrical properties. *J. Manuf. Process.* **2019**, *37*, 339–347. [CrossRef]
41. Moritz, V.F.; Ferreira, C.A.; Devine, D.M. Assessment of ABS/Aluminium composites for 3D printing filaments. In *Proceedings of the IMC37*; Irish Manufacturing Council: Dublin, Ireland, 2021.
42. Farias, N.C.; Major, I.; Devine, D.; Brennan Fournet, M.; Pezzoli, R.; Farshbaf Taghinezhad, S.; Hesabi, M. Multiple recycling of a PLA/PHB biopolymer blend for sustainable packaging applications: Rheology-morphology, thermal, and mechanical performance analysis. *Polym. Eng. Sci.* **2022**, *62*, 1764–1774. [CrossRef]
43. Wang, S.; Capoen, L.; D'hooge, D.R.; Cardon, L. Can the melt flow index be used to predict the success of fused deposition modelling of commercial poly(lactic acid) filaments into 3D printed materials? *Plast. Rubber Compos.* **2018**, *47*, 9–16. [CrossRef]
44. Ferg, E.E.; Bolo, L.L. A correlation between the variable melt flow index and the molecular mass distribution of virgin and recycled polypropylene used in the manufacturing of battery cases. *Polym. Test.* **2013**, *32*, 1452–1459. [CrossRef]
45. Mwania, F.M.; Maringa, M.; van der Walt, J.G. A review of the techniques used to characterize laser sintering of polymeric powders for use and re-use in additive manufacturing. *Manuf. Rev.* **2021**, *8*, 14. [CrossRef]
46. Ghanbari, A.; Mousavi, Z.; Heuzey, M.; Patience, G.S.; Carreau, P.J. Experimental methods in chemical engineering: Rheometry. *Can. J. Chem. Eng.* **2020**, *98*, 1456–1470. [CrossRef]
47. Nikzad, M.; Masood, S.H.; Sbarski, I.; Groth, A. A study of melt flow analysis of an ABS-Iron composite in fused deposition modelling process. *Tsinghua Sci. Technol.* **2009**, *14*, 29–37. [CrossRef]
48. Nikzad, M.; Masood, S.H.; Sbarski, I.; Groth, A.M. Rheological Properties of a Particulate-Filled Polymeric Composite through Fused Deposition Process. *Mater. Sci. Forum* **2010**, *654–656*, 2471–2474. [CrossRef]
49. Sun, Q.; Rizvi, G.M.; Bellehumeur, C.T.; Gu, P. Effect of processing conditions on the bonding quality of FDM polymer filaments. *Rapid Prototyp. J.* **2008**, *14*, 72–80. [CrossRef]

50. Ramanath, H.S.; Chua, C.K.; Leong, K.F.; Shah, K.D. Melt flow behaviour of poly-ε-caprolactone in fused deposition modelling. *J. Mater. Sci. Mater. Med.* **2008**, *19*, 2541–2550. [CrossRef] [PubMed]
51. Liu, B.; Zhang, Y.; Wan, C.; Zhang, Y.; Li, R.; Liu, G. Thermal stability, flame retardancy and rheological behavior of ABS filled with magnesium hydroxide sulfate hydrate whisker. *Polym. Bull.* **2007**, *58*, 747–755. [CrossRef]
52. Galvan, D.; Carneiro, F.; Mazzucco, M.; Bartoli, J.R.; D'Ávila, M.A.; Morales, A.R.; Fernandes, E.G. Effect of Organoclay Mixture on the Rheological Properties of ABS-Clay Nanocomposites. *Macromol. Symp.* **2012**, *319*, 167–172. [CrossRef]
53. Singh, P.; Ghosh, A.K. Torsional, tensile and structural properties of acrylonitrile–butadiene–styrene clay nanocomposites. *Mater. Des.* **2014**, *55*, 137–145. [CrossRef]
54. Gao, C.; Zhang, S.; Wang, F.; Wen, B.; Han, C.; Ding, Y.; Yang, M. Graphene Networks with Low Percolation Threshold in ABS Nanocomposites: Selective Localization and Electrical and Rheological Properties. *ACS Appl. Mater. Interfaces* **2014**, *6*, 12252–12260. [CrossRef]
55. Wei, W.; Hu, S.; Zhang, R.; Xu, C.; Zhang, F.; Liu, Q. Enhanced electrical properties of graphite/ABS composites prepared via supercritical CO2 processing. *Polym. Bull.* **2017**, *74*, 4279–4295. [CrossRef]
56. Ajinjeru, C.; Kishore, V.; Liu, P.; Lindahl, J.; Hassen, A.A.; Kunc, V.; Post, B.; Love, L.; Duty, C. Determination of melt processing conditions for high performance amorphous thermoplastics for large format additive manufacturing. *Addit. Manuf.* **2018**, *21*, 125–132. [CrossRef]
57. Jeong, S.; Song, Y.S.; Lim, E. Fabrication and Characterization of Aluminum Nanoparticle-Reinforced Composites. *Polymers* **2020**, *12*, 2772. [CrossRef] [PubMed]
58. Strano, M.; Rane, K.; Briatico Vangosa, F.; Di Landro, L. Extrusion of metal powder-polymer mixtures: Melt rheology and process stability. *J. Mater. Process. Technol.* **2019**, *273*, 116250. [CrossRef]
59. Hopkins, M.; Gunbay, S.; Hayes, C.; Moritz, V.F.; Fuenmayor, E.; Lyons, J.G.; Devine, D.M. Stereolithography (SLA) utilised to print injection mould tooling in order to evaluate thermal and mechanical properties of commercial polypropylene. *Procedia Manuf.* **2021**, *55*, 205–212. [CrossRef]
60. Chen, J.; Yan, W.; Townsend, E.J.; Feng, J.; Pan, L.; Del Angel Hernandez, V.; Faul, C.F.J. Tunable Surface Area, Porosity, and Function in Conjugated Microporous Polymers. *Angew. Chem. Int. Ed.* **2019**, *58*, 11715–11719. [CrossRef] [PubMed]
61. Kassym, K.; Perveen, A. Atomization processes of metal powders for 3D printing. *Mater. Today Proc.* **2020**, *26*, 1727–1733. [CrossRef]
62. Saheb, S.H.; Durgam, V.K.; Chandrashekhar, A. A review on metal powders in additive manufacturing. *AIP Conf. Proc.* **2020**, *2281*, 020018. [CrossRef]
63. Toby, B.H.; Von Dreele, R.B. GSAS-II: The genesis of a modern open-source all purpose crystallography software package. *J. Appl. Crystallogr.* **2013**, *46*, 544–549. [CrossRef]
64. Rahman, M.; Profili, J.; Moreau, C.; Stafford, L. Formation of self-organized patterns on aluminum substrates by atmospheric pressure plasma jet for surface engineering applications. *Surf. Coat. Technol.* **2022**, *448*, 128919. [CrossRef]
65. Dinaharan, I.; Albert, T. Effect of reinforcement type on microstructural evolution and wear performance of copper matrix composites via powder metallurgy. *Mater. Today Commun.* **2023**, *34*, 105250. [CrossRef]
66. Fu, S.-Y.; Feng, X.-Q.; Lauke, B.; Mai, Y.-W. Effects of particle size, particle/matrix interface adhesion and particle loading on mechanical properties of particulate–polymer composites. *Compos. Part B Eng.* **2008**, *39*, 933–961. [CrossRef]
67. Ozcelik, B.; Ozbay, A.; Demirbas, E. Influence of injection parameters and mold materials on mechanical properties of ABS in plastic injection molding. *Int. Commun. Heat Mass Transf.* **2010**, *37*, 1359–1365. [CrossRef]
68. Kinloch, A.J.; Young, R.J. *Fracture Behaviour of Polymers*; Springer: Dordrecht, The Netherlands, 1995; ISBN 978-94-017-1596-6. [CrossRef]
69. Braga, N.F.; Passador, F.R.; Saito, E.; Cristovan, F.H. Effect of Graphite Content on The Mechanical Properties of Acrylonitrile-Butadiene-Styrene (ABS). *Macromol. Symp.* **2019**, *383*, 1800018. [CrossRef]
70. Ou, Y.; Yang, F.; Yu, Z.-Z. A new conception on the toughness of nylon 6/silica nanocomposite prepared viain situ polymerization. *J. Polym. Sci. Part B Polym. Phys.* **1998**, *36*, 789–795. [CrossRef]
71. Hu, G.; Cao, Z.; Hopkins, M.; Lyons, J.G.; Brennan-Fournet, M.; Devine, D.M. Nanofillers can be used to enhance the thermal conductivity of commercially available SLA resins. *Procedia Manuf.* **2019**, *38*, 1236–1243. [CrossRef]
72. Venkatesh, C.; Chen, Y.; Cao, Z.; Brennan, S.; Major, I.; Lyons, J.G.; Devine, D.M. Influence of extrusion screw speed on the properties of halloysite nanotube impregnated polylactic acid nanocomposites. *J. Polym. Eng.* **2021**, *41*, 499–508. [CrossRef]
73. Roussi, A.T.; Vouvoudi, E.C.; Achilias, D.S. Pyrolytic degradation kinetics of HIPS, ABS, PC and their blends with PP and PVC. *Thermochim. Acta* **2020**, *690*, 178705. [CrossRef]
74. Kumar, P.; Singh, J.; Kumari, N.; Jurail, S.S.; Verma, D.; Maurya, A.K. Study of mechanical and thermal behavior of alkali modified groundnut shell powder reinforced ABS composites. *Polym. Compos.* **2022**, *43*, 4569–4587. [CrossRef]
75. Yu, T.; Ren, J.; Li, S.; Yuan, H.; Li, Y. Effect of fiber surface-treatments on the properties of poly(lactic acid)/ramie composites. *Compos. Part A Appl. Sci. Manuf.* **2010**, *41*, 499–505. [CrossRef]
76. Ervina, J.; Mariatti, M.; Hamdan, S. Mechanical, electrical and thermal properties of multi-walled carbon nanotubes/epoxy composites: Effect of post-processing techniques and filler loading. *Polym. Bull.* **2017**, *74*, 2513–2533. [CrossRef]
77. Greenhalgh, E.S. *Failure Analysis and Fractography of Polymer Composites*, 1st ed.; Woodhead Publishing Ltd.: Cambridge, UK, 2009; ISBN 9781845692179.

78. Torrado, A.R.; Shemelya, C.M.; English, J.D.; Lin, Y.; Wicker, R.B.; Roberson, D.A. Characterizing the effect of additives to ABS on the mechanical property anisotropy of specimens fabricated by material extrusion 3D printing. *Addit. Manuf.* **2015**, *6*, 16–29. [CrossRef]
79. Zheng, Y.; Shen, Z.; Cai, C.; Ma, S.; Xing, Y. Influence of nonmetals recycled from waste printed circuit boards on flexural properties and fracture behavior of polypropylene composites. *Mater. Des.* **2009**, *30*, 958–963. [CrossRef]
80. Carballeira, P.; Haupert, F. Toughening effects of titanium dioxide nanoparticles on TiO2/epoxy resin nanocomposites. *Polym. Compos.* **2009**, *31*, 1241–1246. [CrossRef]
81. Beura, S.; Chakraverty, A.P.; Thatoi, D.N.; Mohanty, U.K.; Mohapatra, M. Failure modes in GFRP composites assessed with the aid of SEM fractographs. *Mater. Today Proc.* **2021**, *41*, 172–179. [CrossRef]
82. Torrado Perez, A.R.; Roberson, D.A.; Wicker, R.B. Fracture Surface Analysis of 3D-Printed Tensile Specimens of Novel ABS-Based Materials. *J. Fail. Anal. Prev.* **2014**, *14*, 343–353. [CrossRef]
83. Ryder, M.A.; Lados, D.A.; Iannacchione, G.S.; Peterson, A.M. Fabrication and properties of novel polymer-metal composites using fused deposition modeling. *Compos. Sci. Technol.* **2018**, *158*, 43–50. [CrossRef]